Journal of Colloid and Interface Science 394 (2013) 100–107

Contents lists available at SciVerse ScienceDirect

Journal of Colloid and Interface Science

www.elsevier.com/locate/jcis

# Controlled synthesis of ceria nanoparticles for the design of nanohybrids

Thanh-Dinh Nguyen [a], Cao-Thang Dinh [a], Driss Mrabet [a], Minh-Nguyet Tran-Thi [b], Trong-On Do [a,*]

[a] Department of Chemical Engineering, Laval University, Quebec, G1V 0A6, Canada
[b] Institute of Materials Science, Vietnam Academy of Science and Technology (VAST), Vietnam

ARTICLE INFO

*Article history:*
Received 19 August 2012
Accepted 9 December 2012
Available online 28 December 2012

*Keywords:*
Nanoparticle
Single-crystalline nanocrystal
Nanocube
Hybrid nanostructure
Catalyst
CO oxidation

ABSTRACT

Ceria nanoparticles were synthesized from reaction mixture of cerium nitrate/hexamethylenediamine/water–ethylene glycol. Lamellar, particle-aggregated array, platelet, rice, cube, quasi-sphere shapes of the ceria nanoparticles can be controlled by tuning reaction parameters (reagent concentration, reagent components, pH, and reaction conditions). Studies on shape-dependent catalysis of the bare ceria samples toward CO oxidation indicated that the cube-shaped ceria nanoparticles show better catalytic activity than the nanospheres and the commercial micropowders. As capped by hexamethylenediamine (HEA) molecules, amine-functionalized ceria nanoparticles act as platforms for depositing copper particles to produce efficient $Cu/CeO_2$ hybrid nanocatalysts for CO conversion. Coupling of the copper clusters with the HEA-capped ceria nanocubes was achieved with the Cu contents up to 15 wt.%. The $Cu/CeO_2$ nanohybrids show an enhanced catalytic efficiency of low temperature CO conversion. This could be due to high exposure of the reactive {1 0 0} facets in the ceria nanocubes and interfacial copper–ceria interactions.


## 1. Introduction

Surfactant-stabilized synthesis has become a powerful paradigm for manipulating uniform shape of inorganic nanoparticles [1–3]. Selective adsorption and capping of the surfactant (capping agent) on the nanoparticles surface allow controlling the growth of the desired particles [4,5]. First developed for the synthesis of the metal, metal oxide, mixed oxide nanoparticles [2,6], the surfactant-stabilized synthesis has been extended to the diverse hybrid nanocomposites [7], that could offer nanotechnological applications [7,8]. By varying the nature and concentration of the capping agent, it has proven possible to tune the shape, the size, and the properties of the inorganic nanoparticles [9,10].

Ceria ($CeO_2$) nanomaterials have been widely established as a principal oxygen carrier used in oxidation catalysis [11,12]. The specific catalytic support is originated from its high oxygen storage capability (OSC) that is associated with rich oxygen vacancies at the ceria surface [13]. The studies on the exposed reactive facet-dependent catalysis of the $CeO_2$ nanocrystals were predicted that the surface reactivity on {1 0 0} facet is considerably higher than that on either {1 1 0} or {1 1 1} [14,15]. These properties lead to synthesize in controlling high exposed percentage of the {1 0 0} facet of the ceria nanocrystals, producing a most active catalytic support [15–17].

Depositing copper particles onto the ceria nanoparticles affords $Cu/CeO_2$ nanohybrids that have been known as an efficient catalyst for CO oxidation [18]. The hybrid nanocomposites typically have synergistic catalytic property arising from particle–particle interactions between the components of such system [7,19]. This concept demonstrated that the copper–ceria interactions occurred in a $Cu/CeO_2$ nanosystem could facilitate the formation of more oxygen vacancies, thus offer an enhanced catalytic activity [20]. Otherwise, the catalytic properties of the nanohybrids are dramatically dependent on the size and the distribution of the deposited metal particles and the exposed reactive facet of the supports [21,22]. Thereby to yield a highly active catalyst for the low temperature CO conversion, small-sized copper particles well-distributed on the reactive facets of the ceria support have been expected.

Recent progress of the surfactant-assisted methods has allowed the controlled synthesis of the ceria nanoparticles with diverse uniform shapes [23,24]. Adschiri et al. [25] reported a hydrothermal two-phase route to synthesize ceria nanocubes through phase-transfer dehydration of cerium hydroxide precursors under supercritical water conditions. The product shape could be controlled by tuning the interaction of organic molecules with various crystallographic planes of the ceria particles. Xia et al. [26] presented the formation of ceria nanosheets through the self-organization of the small particles prepared by adding cerium nitrate to aqueous solution of 6-aminohexanoic acid at 95 °C. Recently, we reported a modified two-phase synthesis of uniform ceria nanocrystals through phase-transfer dehydration of cerium precursors from water to toluene phase [27]. The shape elongation of the ceria nanocubes was achieved with increasing the cerium monomer concentration in the water phase. The use of 6-aminohexanoic acid as water-soluble capping agent allowed us to develop an aqueous-

* Corresponding author. Fax: +1 418 656 5993.
*E-mail address:* trong-on.do@gch.ulaval.ca (T.-O. Do).

0021-9797/$ - see front matter © 2012 Elsevier Inc. All rights reserved.
http://dx.doi.org/10.1016/j.jcis.2012.12.020

solution method for synthesizing cube-shaped ceria nanocrystals dispersed in water [28].

Many attempts have been used the synthesized ceria nanoparticles as platforms for the design of hybrid metal/oxide nanostructures and explored their promising performance in the oxidation catalysis. We recently performed the coupling of the metallic clusters with the oxide nanoparticles to produce the hybrid nanocomposites through seed-mediated growth in assistance of bifunctional organic linker [28], cooperative assemblage [29], photodeposition [30], and ion-exchange deposition [31]. The size-dependent catalysis of the hybrid metal/ceria catalysts was reported by different research groups. For example, Prince et al. [32] loaded Cu particles impregnably on ceria micropowders to produce nanohybrids for low temperature CO conversion, probably due to CO adsorption on the copper in the vicinity of the reactive ceria facets. Lee et al. [33] used the impregnation process to prepare different-shaped ceria nanoparticles and sequential deposition of Cu particles onto the ceria supports for preferential CO oxidation. However, aqueous-solution synthesis of amine-functionalized ceria nanocrystals with diverse shapes for the design of metal/ceria nanohybrids is visually unexplored.

In this paper, we describe a surfactant-assistant pathway to synthesize the ceria nanoparticles in aqueous media. The shape of the ceria nanoparticles could be controlled by changing the synthetic parameters such as reagent concentration, reagent components, pH, and reaction conditions. The use of hexamethylenediamine (HEA) as a biamine-functional linker in the ceria nanoparticles synthesis is crucial for sequential depositing metallic (e.g., copper) particles onto the amine-functionalized ceria supports to afford efficient hybrid nanocatalysts for CO conversion.

## 2. Experimental section

### 2.1. Chemicals

All chemicals were used as received without further purification. Cerium nitrate hexahydrate ($Ce(NO_3)_3{\cdot}6H_2O$, 99%), commercial cerium (IV) oxide micropowder (ceria with particle size <5 μm, 99.9%), copper nitrate ($Cu(NO_3)_2$, 99.99%), ethylene glycol (EG, 99.8%), hexamethylenediamine ($H_2NC_6H_{12}NH_2$, HEA, technical grade, 70% wt.% in 30 v.% $H_2O$), sodium borohydride ($NaBH_4$, >98%) were purchased from Sigma–Aldrich. Sodium hydroxide was purchased from Reagent ACS.

### 2.2. Synthesis of $CeO_2$ nanoparticles

In typical synthesis, an amount (0.03 mol, 13.02 g) of $Ce(NO_3)_3{\cdot}6H_2O$ was added to 10 mL of aqueous HEA solution 1.5 M with the HEA/Ce molar ratio of 1:2 under vigorous stirring and then added 20 mL of aqueous NaOH solution 15 M. The pH value of the reaction mixture was approximately 14. The reaction mixture (30 mL) was transferred to a 50 mL Teflon-lined stainless steel autoclave, heated to 180 °C for 3 days without stirring, and then cooled down naturally to room temperature. The products (noted **C-5** in Table 1) obtained precipitated out of the reaction mixture. The precipitations were filtered out and washed by distilled water for several times to remove impurities. To control the shape of the ceria nanoparticles, the reaction parameters of the synthetic procedure as described above were changed (see Table 1). Increasing the HEA concentration in the bulk mixture with the HEA/Ce molar ratio of 10:1 and 20:1 was obtained the corresponding samples **C-6** and **C-7**, while the other reaction conditions unchanged. To reduce the size of the ceria nanoparticles down to around 10 nm, the cerium nitrate concentration in the synthesis mixture was decreased to 10-fold (0.003 mol; 1.3 g), corresponding to the HEA/Ce molar ratio of 5:1. The samples **C-1**, **C-2**, **C-3**, **C-4** were synthesized using the HEA/Ce ratio of 5:1 at 180 °C with shorter reaction time. Namely, **C-4** was obtained at 180 °C for 24 h using a reaction solvent mixture (pH 14) of 20 mL water and 10 mL EG. **C-3** was obtained at 180 °C for 24 h using only EG as reaction medium (pH 7). Starting with a reaction solvent mixture of 20 mL water and 10 mL EG, keeping the HEA/Ce ratio of 5:1 and pH 14, hydrothermal treatment of the reaction mixture in an autoclave at 180 °C for 24 h obtained **C-2**. Heating the reaction mixture in a flask at 180 °C with a stirring speed of 3000 rpm for 30 min under atmospheric pressure was obtained **C-1**.

### 2.3. Preparation of $Cu/CeO_2$ nanohybrids

An aqueous $Cu(NO_3)_2$ solution (5 mL, 31.2–93.6 mM) was added to 5 mL of an aqueous $CeO_2$ nanocube suspension (0.2 g of the ceria nanoparticle powders, **C-5**) under continuous stirring. The $Cu^{2+}$ ions dispersed in the ceria particles suspension were reduced to metallic copper particles by adding 10 mL of freshly aqueous $NaBH_4$ solution (46.8–140.4 mM) under stirring at ambient conditions. The pH value of the reaction mixture before reduction was ~7. The loading content of the metallic copper particles was varied ranging from 5 to 15 wt.%. Within 4 h, the color of the reaction mixture changed to light brown, indicating the formation of the metallic Cu species. The precipitated particles were collected and washed with distilled water for several times to remove impurities and dried at 60 °C for 2 h. The capped $Cu/CeO_2$ nanohybrids were calcined under air at a heating rate of 2 °C $min^{-1}$ up to 300 °C, held at this temperature for 2 h, then heated to 550 °C at 2 °C $min^{-1}$, and then held at this temperature for 3 h.

### 2.4. Characterization

Powder X-ray diffraction (PXRD) patterns were recorded on a Bruker SMART APEXII X-ray diffractometer using Cu Kα radiation ($\lambda$ = 1.5418 Å). Transmission electron microscope (TEM) images and selected area electron diffraction (SAED) of the samples were obtained on a JEOL JEM 1230 operated at 120 kV. The samples were prepared by placing one drop (0.1 mL) of the diluted ethanol solution of the nanoparticles onto a 200 mesh carbon-coated copper

**Table 1**
Different preparation conditions for shape-controlled ceria nanocrystals.

| Sample | $Ce^{3+}$ (mol) | HEA (mol) | Water (mL) | EG (mL) | pH | Reaction conditions | Morphology-size (nm) |
|---|---|---|---|---|---|---|---|
| **C-1** | 0.003 | 0.015 | 20 | 10 | 7 | 180 °C, 30 min[a] | Lamellar |
| **C-2** | 0.003 | 0.015 | 20 | 10 | 7 | 180 °C, 24 h | Particle array |
| **C-3** | 0.003 | 0.015 | 0 | 30 | 7 | 180 °C, 24 h | Platelet-rod |
| **C-4** | 0.003 | 0.015 | 20 | 10 | 14 | 180 °C, 24 h | 6–10 nm rice |
| **C-5** | 0.030 | 0.015 | 30 | 0 | 14 | 180 °C, 3 d | 120 nm cube |
| **C-6** | 0.030 | 0.300 | 30 | 0 | 14 | 180 °C, 3 d | 40 nm cube |
| **C-7** | 0.030 | 0.600 | 30 | 0 | 14 | 180 °C, 3 d | 40 nm sphere |

[a] The sample was synthesized in a flask under atmospheric pressure. The other samples were synthesized in an autoclave.

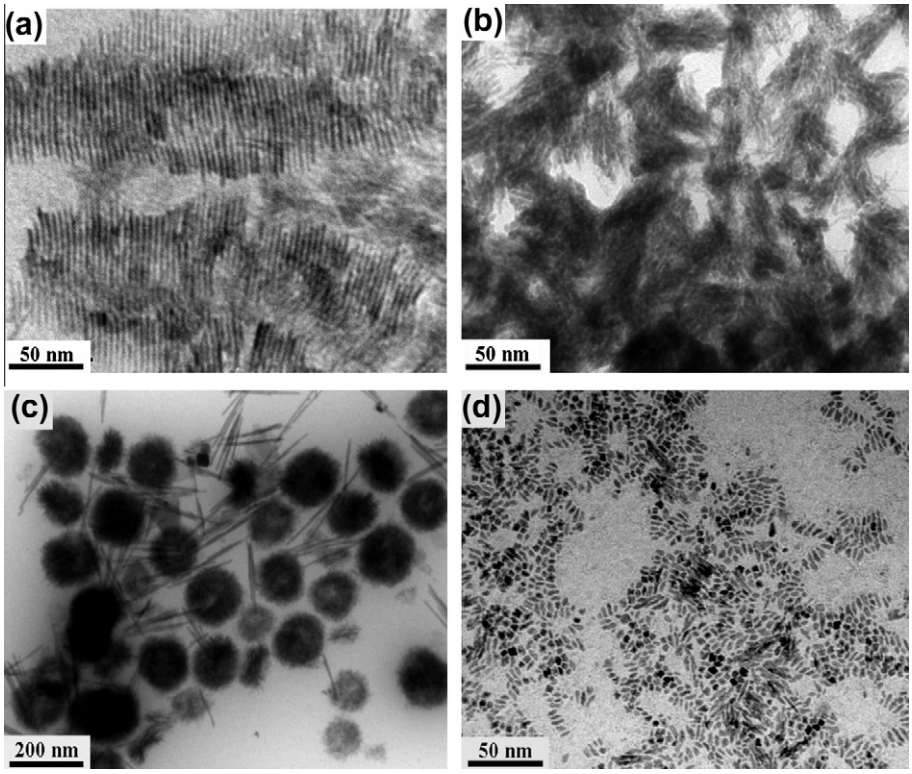


**Fig. 1.** TEM images of ceria nanoparticles formed through surfactant-stabilized synthesis in controlling the shape by changing the reaction parameters shown in Table 1: (a) **C-1**, (b) **C-2**, (c) **C-3** and (d) **C-4**.

grid and dried at ambient conditions. Particle size distribution histograms were obtained from statistical treatment of TEM image by measuring the diameter of ~30 particles using ImageJ software. Average particle diameters were determined from this particle size distribution histogram. Theoretical surface area calculated from TEM average particle size: $S_{th} = 6000/(\rho d)$, where $\rho$ and $d$ are the material density ($\rho_{Ceria} = 7.65\ g\ cm^{-3}$ and $\rho_{Copper} = 8.92\ g\ cm^{-3}$) and particle diameter (nm) estimated from particle size distribution histogram of TEM image, respectively. Energy-dispersive X-ray (EDX) analysis was collected using a JEOL 6360 scanning electron microscope. X-ray photoelectron spectroscopy (XPS) was carried out in an ion-pumped chamber (evacuated to $10^{-9}$ Torr) of a photoelectron spectrometer (Kratos Axis-Ultra) equipped with a focused X-ray source (Al K$\alpha$, $h\nu = 1486.6$ eV). The binding energy of the samples was calibrated by setting the C 1s peak to 285 eV. Thermogravimetric (TGA) analysis of the HEA-capped ceria nanoparticles (~5 mg) was carried out at a heating rate of 10 °C $min^{-1}$, under an air flux up to 600 °C using a Perkin–Elmer TGA thermogravimetric analyzer. Fourier transform infrared (FTIR) spectroscopy was measured with FTS 45 infrared spectrophotometer with KBr pellet technique. Nitrogen adsorption–desorption isotherms obtained using Quantachrome Autosorb-1 system; before measurements, the samples (~120 mg) were degassed at 150 °C in vacuum for 4 h.

### 2.5. Catalytic test

The catalytic tests for CO conversion were carried out in a quartz tubular continuous flow microreactor under steady-state conditions at atmospheric pressure and different temperatures. The catalytic activity of the $Cu/CeO_2$ catalysts was compared to the $CeO_2$ nanospheres and the commercial 50–80 nm $CeO_2$ powders as a reference catalyst. An amount (120 mg) of the catalysts calcined at 550 °C for 3 h was diluted with the same amount of glass beads (20–40 mesh size) and loaded inside a fixed-bed-U-shaped tubular quartz reactor with internal diameter of 4.0 mm between two zones of glace wool. The reactor was placed in a cylindrical electric furnace, and a thermocouple was inserted into the catalyst bed to monitor its internal temperature. The catalysts were activated by passing a flow with 30 mL $min^{-1}$ of dried ultrapure He at 250 °C and subsequent the use of a mixture of $H_2$/He (10% $H_2$). The catalytic activity of catalysts toward CO oxidation was carried out in a continuous flow reactor. A stream of 60 mL $min^{-1}$ reaction gas mixture containing 2.3% CO, 2.5% $O_2$, and the balance He was passed on the catalyst bed at different temperatures for specified times. Catalytic activity was measured at different temperatures with the reaction temperature rising from room temperature to 500 °C in step of 20 °C. The composition of the influent and effluent gas was analyzed by an online HP 5890 gas chromatograph equipped with a carboxen-1010 PLOT column and a thermal conductivity detector (TCD) detector. The CO conversion was calculated from the change in CO concentration in the inlet and the outlet gases using the calibration curve.

## 3. Results and discussion

Ceria nanoparticles were synthesized through aqueous-solution pathway using cerium nitrate as precursor, HEA as capping agent, and water or water–ethylene glycol as synthetic media. Upon heating, cerium precursors transformed to cerium hydroxide monomers and dehydrated to ceria nuclei, whose subsequent growth to nanoparticles capped by HEA molecules. After the synthesis, the capped nanoparticle products precipitated out of the reaction mixture. The influences of the synthetic parameters on the shape of the ceria nanoparticles were studied by altering reagent concentration, reagent components, pH, and reaction conditions shown in Table 1. The amine-functionalized ceria nanoparticles were used as

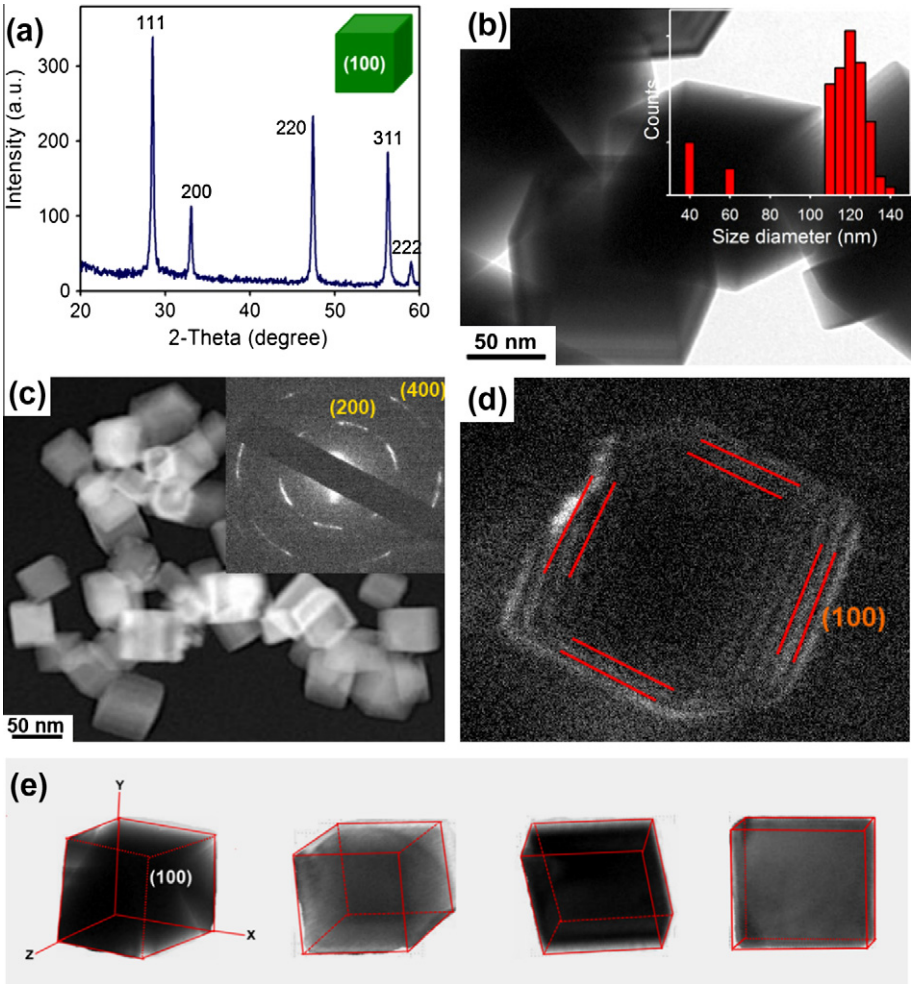


**Fig. 2.** Ceria nanocubes synthesized with HEA/Ce molar ratio of 1:2 (**C-5**). (a) PXRD. (b) TEM, inset of histogram of particle size distribution. (c) Dark-field TEM. (d) SAED patterns and inset of c. (e) TEM images of a single nanocube taken at the different orientations.

nanosupports for the design of metal/ceria nanohybrids. This chemistry method is simple and highly reproducible, inexpensive reagents, and aqueous reaction media used.

Fig. 1 shows different shapes of the ceria nanoparticles prepared by varying the reaction parameters. Starting with an aqueous reaction mixture of 0.003 mol (1.3 g) cerium nitrate, 0.015 mol HEA molecules (HEA/Ce ratio of 5:1), if adding 10 mL ethylene glycol (EG) to the aqueous reaction mixture (20 mL), the reaction mixture was poured in a flask and heated at 180 °C for 30 min under atmospheric pressure to yield the product (**C-1** in Table 1). A representative TEM image of **C-1** in Fig. 1a shows a quite uniform ceria layered nanostructure constituted equally spaced parallel lamellar with 10 nm in the width and 50–200 nm in the length. Small-angle PXRD pattern (Fig. S1A) of **C-1** shows two diffraction peaks indexed as (001) and (002) reflections of a lamellar nanophase, suggesting that the biamine-functional HEA capping agents could be arranged as bilayers between the capped ceria layers to form the ceria lamellar nanostructures under atmospheric pressure. Otherwise, the synthetic procedure proceeded under autoclave-generated pressure favored the formation of the ceria nanoparticles. Namely, the reaction mixture was transferred into an autoclave and heated at 180 °C for 24 h; aggregated arrays (**C-2**) composed of 2–4 nm-sized ceria particles were formed (Fig. 1b). When only EG was used as reaction medium without water, while the other synthetic conditions unchanged, a mixture of platelet- and rod-shaped ceria nanoparticles (**C-3**) was produced (Fig. 1c). The platelet-shaped architectures with the size of 180 nm are made up of densely packed clusters. The formation of the cluster-aggregated platelets might cause the slow growth of the ceria crystals in high viscous environment of EG solvent [34]. If increasing the pH value of the reaction mixture of cerium nitrate/HEA/water–EG from 7 to 14, while keeping the same synthesis conditions (the hydrothermal process in an autoclave at 180 °C for 24 h), 6–10 nm-sized ceria nanorices (**C-4**) were obtained (Fig. 1d). The rapid dehydration of the cerium ions in basic media might facilitate the fast growth of the ceria nuclei, thus gave the rice-shaped nanocrystals, instead of the cluster aggregates formed in mixed water–ethylene glycol media. The cubic-phase structure of the ceria nanoparticles (**C2**, **C3**, **C4**) synthesized under autoclave-generated pressure was confirmed by wide-angle PXRD spectra shown in Fig. S1B.

When only water was used as reaction medium, without EG, and with increasing the cerium nitrate concentration to 10-fold (0.03 mol, 13.02 g), the hydrothermal aging on the reaction mixture of cerium nitrate/HEA/water (pH ~ 14) with the HEA/Ce molar ratio of 1:2 for 3 days in an autoclave at 180 °C produced single-crystalline ceria nanocrystals (**C-5**). We found that the molar ratio of the HEA molecules relative to the cerium precursor is an important role in determining the shape of the ceria nanocrystals. Thus, the experiments were performed with variable HEA concentrations (including one preparation without HEA). The hydrothermal treatment of the reaction mixture without HEA afforded a mixture of nanocubes and irregular particles with a broad population

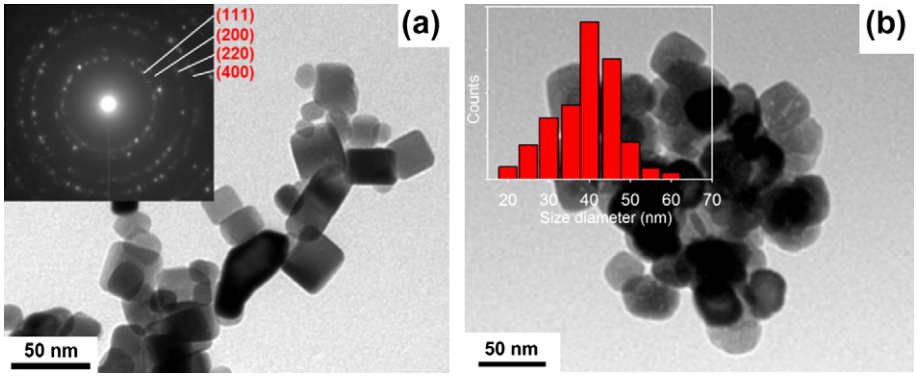


**Fig. 3.** TEM images of ceria nanocrystals synthesized using different HEA/Ce molar ratios: (a) HEA/Ce of 10:1, **C-6** and (b) HEA/Ce of 20:1, **C-7**, inset of PSD histogram shown a narrower distribution.

(Fig. S2). Fig. 2 shows PXRD, TEM, and SAED patterns of **C-5**. The PXRD spectrum (Fig. 2a) exhibits intense diffraction peaks assigned to (111), (200), (220), (311) planes, characteristic of a cubic phase and high crystallinity (*Fm*3*m*, JCPDS 34-0394) [17]. There are not any other impurities of cerium (III) hydroxide structure detected. As seen in Fig. 2b and Fig. S3, TEM images show single-crystalline and well-shaped ceria nanocubes with average edge length of 120 nm. The projection views of the almost particles are perfect square shape, clear-cut edge, and smooth surface without obvious defects. Particle size distribution (PSD) histogram of **C-5** obtained from statistical treatment of particle diameters from the TEM image shows that the product is composed of ~80% 120 nm cube-shape particles and ~20% 40–60 nm nanoparticles.

As seen in Fig. 2c, the single crystallinity of the nanocubes was verified by both dark-field TEM image and electron diffraction taken over a large domain (Fig. 2d). SAED pattern (inset of Fig. 2c) taken by focusing the electronic beam at one point on a ceria nanocube reveals only detectable diffraction rings of (200) and (400) display an enhanced brightness, indicating that the six surfaces of a single-crystalline ceria nanocube are terminated with selectively growth of the {100} facets [17]. Panel e in Fig. 2 shows four free-standing single 3-dimensional nanocubes displayed four differently projected shapes under TEM, depending on its orientations relative to the electron beam. Each cube has six well-defined {100} facets exposed, whose the surface energy could be considered as the highest among {110} and {111} facets [14,15]. When varying the HEA/Ce molar ratio from 1:2 (**C-5**) to 10:1 (**C-6**), and 20:1 (**C-7**), the particle size reduced from 120 to 40 nm, and their shape gradually transformed from mixed nanocube and polyhedron into quasi-nanosphere (Fig. 3a and b). The SAED pattern (inset of Fig. 3a) of **C-6** shows distinct diffraction spots of (111), (200), (220), (400) planes, instead of only the (200) and (400) rings appeared in the 120 nm nanocube indicative of the formation of the ceria nanocrystals with mixed cubic-, polyhedral, spherical-like shapes [17]. At low HEA concentration, the formation of the ceria nanocubes could result in blocking the {100} facets by amine groups of the HEA molecules, and the selective growth along these facets was considerably restricted. A decrease in the particle size along with transformating to the isotropic shape at the high HEA concentrations could be relevant to a high fraction of surfactant protection at the ceria surface.

The formation of the {100}-faceted ceria nanocubes (**C-5**) at the high precursor monomer concentration could result in the coalescence of the formed ceria crystals. Fig. S3 shows representative TEM images of the ceria samples synthesized at 180 °C for different lengths of reaction time (1–3 days) with the same initial chemical compositions used. At a short stage (1 day), numerous particles with sizes of less than 20 nm emerged, and some of them coalesced into large particles with sizes of 50–70 nm (Fig. S4a). The primary particles had a tendency to disappear gradually with prolonged

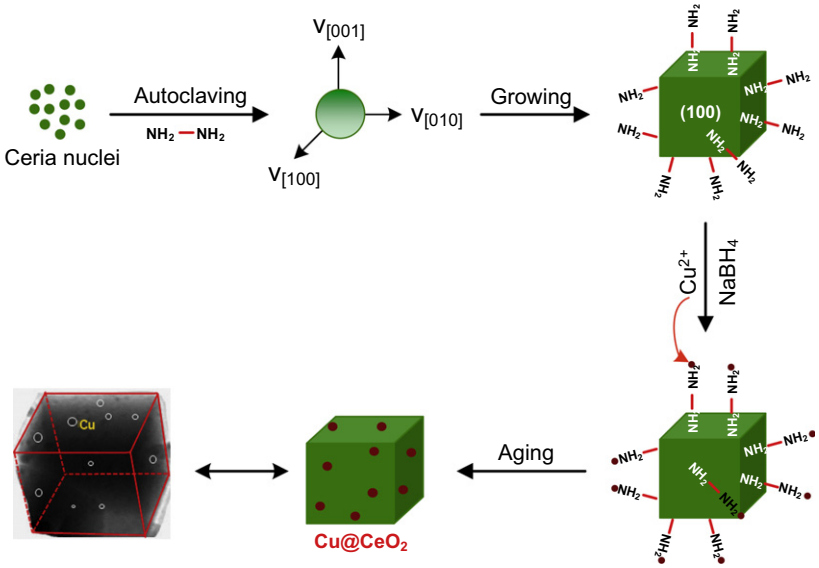


**Scheme 1.** A possible scheme for the formation of single-crystalline $CeO_2$ nanocubes for the design of Cu/$CeO_2$ hybrid nanostructures.

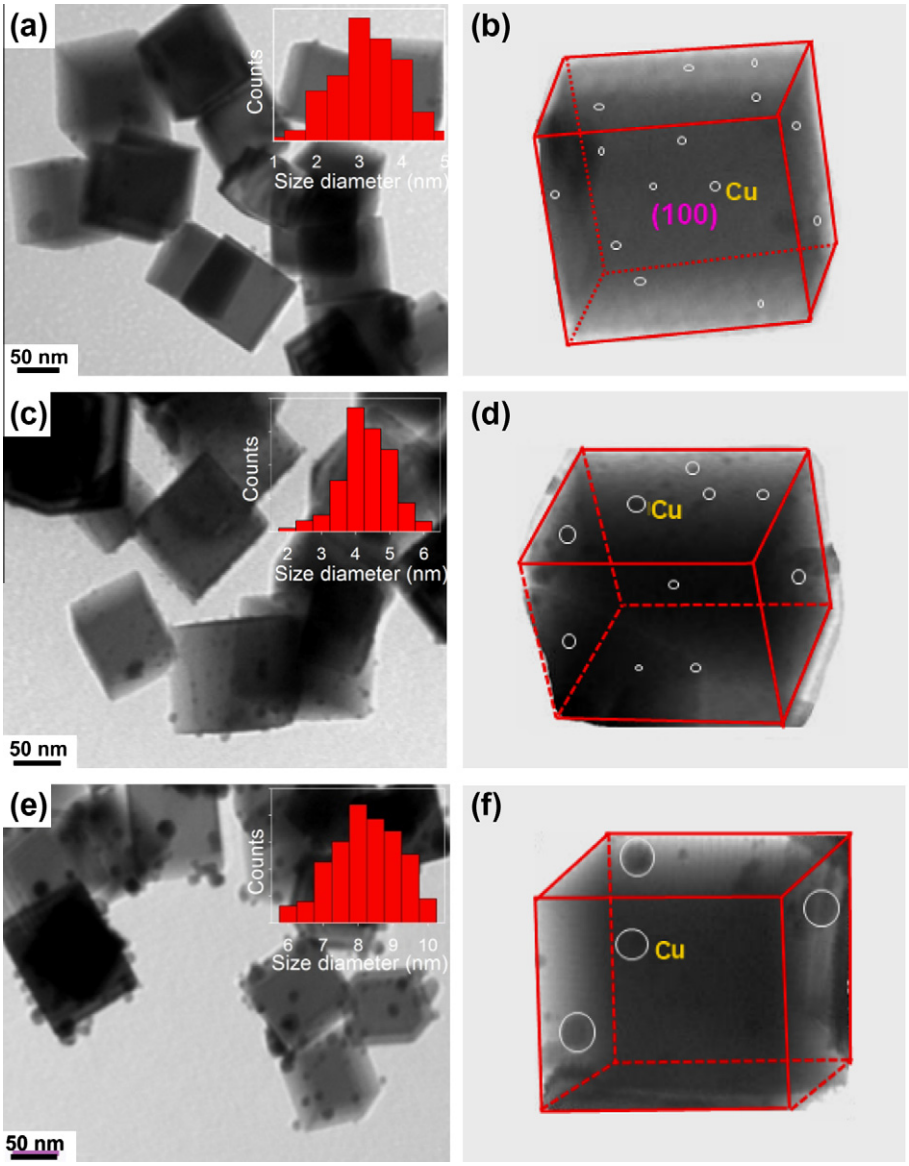


**Fig. 4.** Effect of copper contents (wt.%) on the size (*d*, nm) of Cu particles onto the {100}-faceted ceria nanocubes (**C-5**). TEM images of the hybrid samples and inset of PSD histograms of the deposited Cu particles: 4.9 Cu wt.%, *d* = 2–3 nm (a and b), 9.1 Cu wt.%, *d* = 4–5 nm (c and d) and 13.8 Cu wt.%, *d* = 7–9 nm (e and f).

reaction time (2 days), and the large particles kept growing by probably means of the surface attachment and subsequent recrystallization (Fig. S4b). The well-shaped nanocubes (**C-5**) with large size of ~120 nm were dominantly formed after 3 days (Fig. 1b–e, Fig. S3). The fusing event could be considered by Ostwald ripening process for which the primary particles act as seeds for the direct growth of the ceria monomers [35].

Defective surface structures of the ceria nanoparticles are an essential role in oxidation catalysis [27]. This property is determined by XPS to confirm the percentage of $Ce^{3+}$ surface concentration in the ceria nanoparticles. The XPS results of **C-5** and **C-7** show that Ce 3d XPS spectra (Fig. S5) of both the samples exhibit two oxidation states of $Ce^{3+}$ and $Ce^{4+}$. The percentage of $Ce^{3+}$ in **C-5** (18% area) is however higher than in **C-7** (12% area), demonstrating that the fraction of $Ce^{3+}$ mainly depends on the shape of the ceria nanoparticles. The highly exposed reactive {100} facets in the ceria nanocubes (**C-5**) may contain more unsaturated coordination of cerium atoms than other facets in the quasi-nanospheres (**C-7**), which could improve the catalytic properties. TGA profile (Fig. S6) of **C-5** shows a steep weight loss of ~1 wt.%, appearing around 200–450 °C, assigning to decomposition of the HEA molecules. An amount of the HEA capped on the ceria surface is as low as ~1 wt.%, due to the low HEA/Ce ratio of 1:2 used in the synthesis mixture. A gradual mass gain of the ceria materials (~0.4 wt.%) observed above 450 °C could cause the oxidation of $Ce^{3+}$ to $Ce^{4+}$ occurred at the ceria surface indicative of the defected structure in good agreement with the XPS results. FTIR spectrum (Fig. S7) of **C-5** shows the N–H stretching bands at 1465–1665 $cm^{-1}$ of amino groups of the HEA molecules [34]. C 1s and N 1s XPS spectra (Fig. S5b and c) of **C-5** were also detected. An O 1s XPS peak (Fig. S5d) was observed at 531.5 eV associated with hydroxide groups located on the ceria surface.

As capped by the HEA molecules, the amine-functionalized ceria nanoparticles are effective platforms for the design of hybrid metal (e.g., copper)/ceria nanostructures. The $Cu^{2+}$ ions dispersed in the amine-functionalized ceria particle suspension were reduced to metallic Cu particles by freshly aqueous $NaBH_4$ solution. A possible scheme for the formation of the $Cu/CeO_2$ nanohybrids is expressed in Scheme 1. The size of the Cu particles onto the ceria nanoparticles can be controlled by adjusting the $Cu^{2+}$ concentra-

tion in the aqueous synthetic mixture. In this current work, we have selected the 120 nm-sized ceria nanocubes (**C-5**) as a typical example to clarify the nanohybrid formation.

Coupling of the copper clusters with the ceria nanocubes (**C-5**) to produce the $Cu/CeO_2$ nanohybrids was achieved at initial Cu contents ranging from 5 to 10 and 15 wt.%, corresponding to ~4.9, 9.1, 13.8 wt.% in the calcined $Cu/CeO_2$, as determined by EDX spectra (Fig. S11c). This could predict that the metallic coppers preferentially adsorbed to the exposed amine groups of the HEA molecules capped onto the nanoceria. No significant difference of the Cu content before and after calcination suggests that the copper species were mostly migrated onto the ceria surface, instead of incorporating into the ceria lattice. Fig. 4a–f shows TEM images of the $Cu/CeO_2$ nanohybrids with different copper loadings and inset of PSD histograms of the deposited Cu nanoparticles, which expressed the deposited 3D cubes viewed along the different directions. The overall Cu particles are epitaxial protrusions on the {100} facets and the edges of the ceria nanocubes. The aggregation of the Cu particles separately aside from the supported ceria nanocubes was insignificant. At low copper concentration (5 wt.%), 2–4 nm Cu particles were formed onto the ceria nanocube surface (Fig. 4a and b). When increasing the Cu loading to 10 wt.%, a well distribution of 4–5 nm Cu particles was observed (Fig. 4c and d). With the higher Cu loading (15 wt.%), the Cu particles with larger particle size (7–9 nm) accompanied by the coalescence were observed (Fig. 4e and f). Theoretical surface area of the 7–9 nm Cu particles (84.0 $m^2 g^{-1}$) is lower than those of the 4–5 nm Cu particles (149.5 $m^2 g^{-1}$) and 2–4 nm Cu particles (224.0 $m^2 g^{-1}$). Calcination of the capped $Cu/CeO_2$ hybrids at 550 °C under air to remove the HEA linkers afforded hybrid catalysts. The size of Cu particles and the shape of $CeO_2$ supports in the calcined nanohybrids still retain without aggregates (Fig. S8). BET specific surface area (Fig. S9) of the calcined $Cu/CeO_2$ is ~10 $m^2 g^{-1}$, closed to theoretical surface area calculated from the TEM average particle size (~6.5 $m^2 g^{-1}$). The copper particles deposited onto the ceria nanocubes in the calcined hybrids were analyzed by PXRD, EDX, and XPS techniques. The metallic copper and partial copper oxide species (4.9–13.8 wt.%) were unable to detect by PXRD (Fig. S10), probably due to their low crystallinity, high dispersion, and small particle size (Fig. S9). XPS and EDX spectra (Fig. S11) of the calcined $Cu/CeO_2$ provide an evidence of the existence of the Cu species in the calcined hybrid materials. Cu 2p XPS spectrum (Fig. S11b) shows a Cu $2p_{3/2}$ peak at 932.4 eV associated with a mixture of $Cu^\circ$ and partial $Cu^+$ species formed in the hybrid nanostructures [36].

Catalytic activity of the $Cu/CeO_2$ catalysts for CO oxidation was tested in comparison with the bare $CeO_2$ samples. The evolution of the CO conversion over the different catalysts as a function of temperature is presented in Fig. 5. For the bare $CeO_2$ samples with various sizes and shapes, the half CO conversion (50%) was at 410 °C for commercial 50–80 nm $CeO_2$ powders and at 340 °C for the 40 nm $CeO_2$ quasi-nanospheres (synthesized using the HEA/Ce molar ratio of 20:1), while the 120 nm $CeO_2$ nanocubes achieved the half CO oxidation conversion (50%) at a lower temperature (300 °C). In comparison, theoretical surface area of the ceria quasi-nanospheres (19.5 $m^2 g^{-1}$) is higher than those of the ceria nanocubes (6.5 $m^2 g^{-1}$) and the commercial 50–80 nm ceria powders (~14 $m^2 g^{-1}$). The nanocubes have better catalytic efficiency than the nanospheres even though their lower surface area. The XPS results illustrated that the cube-shaped ceria nanostructure is more defective surface than the ceria quasi-nanospheres. This behavior is a crucial factor for improving the catalytic activity because the ceria nanocubes may contain more coordination of unsaturated cerium atoms and more active adsorption of dissociated oxygen species on their highly exposed reactive {100} facets. These results are comparable with Zheng and his co-worker's report on the CO catalytic properties of ceria nanocubes and truncated octahedra [37]. Due to the large-sized ceria nanocubes of ~120 nm, the absence of the mass and heat transfer limitation for the CO conversion was found to be up to ~30% in these catalytic test conditions. For the $Cu/CeO_2$ nanocube catalysts, the 100% CO conversion was reached at 200 °C for the 9.1 wt.% $Cu/CeO_2$, at 225 °C for the 4.9 wt.% $Cu/CeO_2$, and at 300 °C for the 13.8 wt.% $Cu/CeO_2$. The catalytic activity of the 9.1 wt.% $Cu/CeO_2$ is higher than that of the 4.9 wt.% $Cu/CeO_2$ and 13.8 wt.% $Cu/CeO_2$ samples indicative of the Cu particle size-dependent catalysis. The catalytic efficiency of all of the $Cu/CeO_2$ catalysts is much higher than that of the bare ceria. This enhancement could be attributed to the interfacial copper–ceria interactions that might facilitate the formation and migration of more oxygen vacancies in the hybrid nanostructures [38,39].

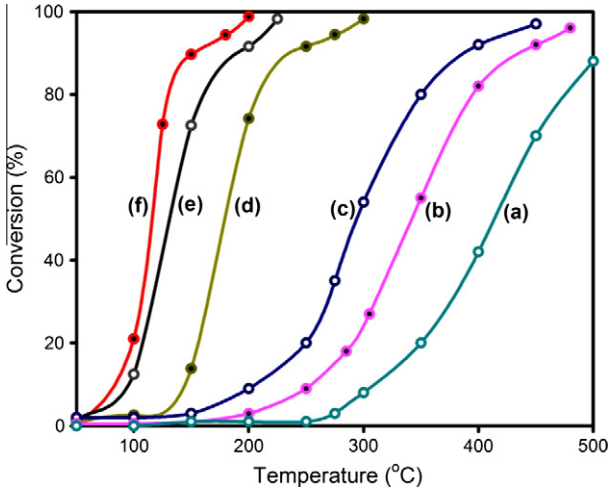


**Fig. 5.** CO conversion as a function of temperature for bare $CeO_2$: (a) commercial 50–80 nm $CeO_2$ powders, (b) 40 nm $CeO_2$ quasi-nanospheres (**C-7**), (c) 120 nm $CeO_2$ nanocubes (**C-5**); for hybrid $Cu/CeO_2$ cubes (Cu/**C-5**): (d) 13.8 wt.% $Cu/CeO_2$, (e) 4.9 wt.% $Cu/CeO_2$ and (f) 9.1 wt.% $Cu/CeO_2$.

## 4. Conclusions

In conclusion, we have demonstrated a surfactant-assistant route for the aqueous-solution synthesis of shape-controlled ceria nanoparticles through thermal treatment of reaction mixture of cerium nitrate/hexamethylenediamine/water–ethylene glycol. Through varying reaction parameters such as reagent concentration, reagent components, pH, and reaction conditions, lamellar, particle-aggregated array, platelet, rice, cube, quasi-sphere shapes of the ceria nanoparticles were obtained. Biamine-functional linker, hexamethylenediamine, plays an important role in controlling the shape of the ceria nanoparticles and then designing hybrid nanocomposites. Size/shape-dependent catalytic activity of the $CeO_2$ nanoparticles was demonstrated; cubic-shaped $CeO_2$ nanocrystals enclosed by {100} facets show better CO catalytic activity than quasi-nanospheres and micropowders. The amine-functionalized ceria nanoparticles were used as platforms for the direct growth of copper particles to produce efficient $Cu/CeO_2$ hybrid nanocatalysts with different Cu contents (up to 15 wt.%) for CO conversion. An enhanced catalytic efficiency of the $Cu/CeO_2$ hybrid nanocatalysts compared to the bare ceria particles could result in high exposure of the reactive {100} facets in the ceria nanocubes and interfacial copper–ceria interactions. The current work supposes that the amine-functionalized $CeO_2$ nanoparticles could provide intermediate sites for attaching secondary species to prepare diverse hybrid-based oxygen carrier nanomaterials.

## Acknowledgment

This work was supported by the Natural Sciences and Engineering Research Council of Canada (NSERC) through a strategic grant.

## Appendix A. Supplementary material

Supplementary data associated with this article can be found, in the online version, at http://dx.doi.org/10.1016/j.jcis.2012.12.020.

## References

[1] M. Niederberger, Acc. Chem. Res. 40 (2007) 793.
[2] J. Park, J. Joo, S.G. Kwon, Y. Jang, T. Hyeon, Angew. Chem. Int. Ed. 46 (2007) 4630.
[3] S.C. Glotzer, Nature 481 (2012) 450.
[4] Y. Xia, Y. Xiong, B. Lim, S.E. Skrabalak, Angew. Chem. Int. Ed. 48 (2009) 60.
[5] Y.W. Jun, J.S. Choi, J. Cheon, Angew. Chem. Int. Ed. 45 (2006) 3414.
[6] A.R. Tao, S. Habas, P. Yang, Small 4 (2008) 310.
[7] R. Costi, A.E. Saunders, U. Banin, Angew. Chem. Int. Ed. 49 (2010) 4878.
[8] A.L.M. Reddy, S.R. Gowda, M.M. Shaijumon, P.M. Ajayan, Adv. Mater. (2012), http://dx.doi.org/10.1002/adma.201104502.
[9] M.A. El-Sayed, Acc. Chem. Res. 37 (2004) 326.
[10] C. Burda, X. Chen, R. Narayanan, M.A. El-Sayed, Chem. Rev. 105 (2005) 1025.
[11] D. Wang, Y. Kang, V.D. Nguyen, J. Chen, R. Kungas, N.L. Wieder, K. Bakhmutsky, R.J. Gorte, C.B. Murray, Angew. Chem. Int. Ed. 50 (2011) 4378.
[12] C.T. Campbell, C.H.F. Peden, Science 309 (2005) 713.
[13] A. Migani, G.N. Vayssilov, S.T. Bromley, F. Illas, K.M. Neyman, J. Mater. Chem. 20 (2010) 10535.
[14] D.C. Sayle, S.A. Maicaneanu, G.W. Watson, J. Am. Chem. Soc. 124 (2002) 11429.
[15] D.C. Sayle, X. Feng, Y. Ding, Z.L. Wang, T.X.T. Sayle, J. Am. Chem. Soc. 129 (2007) 7924.
[16] Q. Fu, H. Saltsburg, M.F. Stephanopoulos, Science 301 (2003) 935.
[17] S. Yang, L. Gao, J. Am. Chem. Soc. 128 (2006) 9330.
[18] C.S. Polster, C.D. Baertsch, Chem. Commun. (2008) 4046.
[19] U. Banin, Nat. Mater. 6 (2007) 625.
[20] A. Tschope, J.Y. Ying, Y.M. Chiang, Mater. Sci. Eng. A 204 (1995) 267.
[21] A. Cao, G. Veser, Nat. Mater. 9 (2010) 75.
[22] H. Zhang, T. Watanabe, M. Okumura, M. Haruta, N. Toshima, Nat. Mater. 11 (2012) 49.
[23] Q. Yuan, H.H. Duan, L.L. Li, L.D. Sun, Y.W. Zhang, C.H. Yan, J. Colloid Interface Sci. 335 (2009) 151.
[24] T. Yu, J. Joo, Y.I. Park, T. Hyeon, Angew. Chem. 117 (2005) 7577.
[25] J. Zhang, S. Ohara, M. Umetsu, T. Naka, Y. Hatakeyama, T. Adschiri, Adv. Mater. 19 (2007) 203.
[26] T. Yu, B. Lim, Y. Xia, Angew. Chem. Int. Ed. 49 (2010) 4484.
[27] T.D. Nguyen, T.O. Do, J. Phys. Chem. C 113 (2009) 11204.
[28] T.D. Nguyen, C.T. Dinh, T.O. Do, Nanoscale 3 (2011) 1861.
[29] D. Mrabet, M.H. Zahedi-Niaki, T.O. Do, J. Phys. Chem. C 112 (2008) 7124.
[30] C.T. Dinh, T.D. Nguyen, F. Kleitz, T.O. Do, ACS Appl. Mater. Interfaces 3 (2011) 2228.
[31] C.T. Dinh, Y. Seo, T.D. Nguyen, F. Kleitz, T.O. Do, Angew. Chem. Int. Ed. 51 (2012) 6794.
[32] V. Matolin, L. Sedlacek, I. Matolinova, F. Sutara, T. Skala, B. Smid, J. Libra, V. Nehasil, K.C. Prince, J. Phys. Chem. C 112 (2008) 3751.
[33] J. Han, H.J. Kim, S. Yoon, H. Lee, J. Mol. Catal. A: Chem. 335 (2011) 82.
[34] T.D. Nguyen, D. Mrabet, T.T.D. Vu, C.T. Dinh, T.O. Do, CrystEngComm. 13 (2011) 1450.
[35] J. Yin, Z. Yu, F. Gao, J. Wang, H. Pang, Q. Lu, Angew. Chem. 122 (2010) 6472.
[36] B.L. Gustafson, P.S. Wehner, Appl. Surf. Sci. 52 (1991) 261.
[37] X. Wang, Z. Jiang, B. Zheng, Z. Xie, L. Zheng, CrystEngComm. 14 (2012) 7579.
[38] J. Beckers, G. Rothenberg, Dalton Trans. (2008) 6573.
[39] J. Qin, J. Lu, M. Cao, C. Hu, Nanoscale 2 (2010) 2739.

# Supporting Information

## Controlled Synthesis of Ceria Nanoparticles for the Design of Nanohybrids

**Thanh-Dinh Nguyen, Driss Mrabet, Cao-Dinh Thang, Trong-On Do**

*Department of Chemical Engineering, Laval University, Quebec G1K 7P4 Canada*

Address correspondence to Trong-On.Do@gch.ulaval.ca

Submited to **Journal of Colloid and Interface Science**

*Revised* November 2012

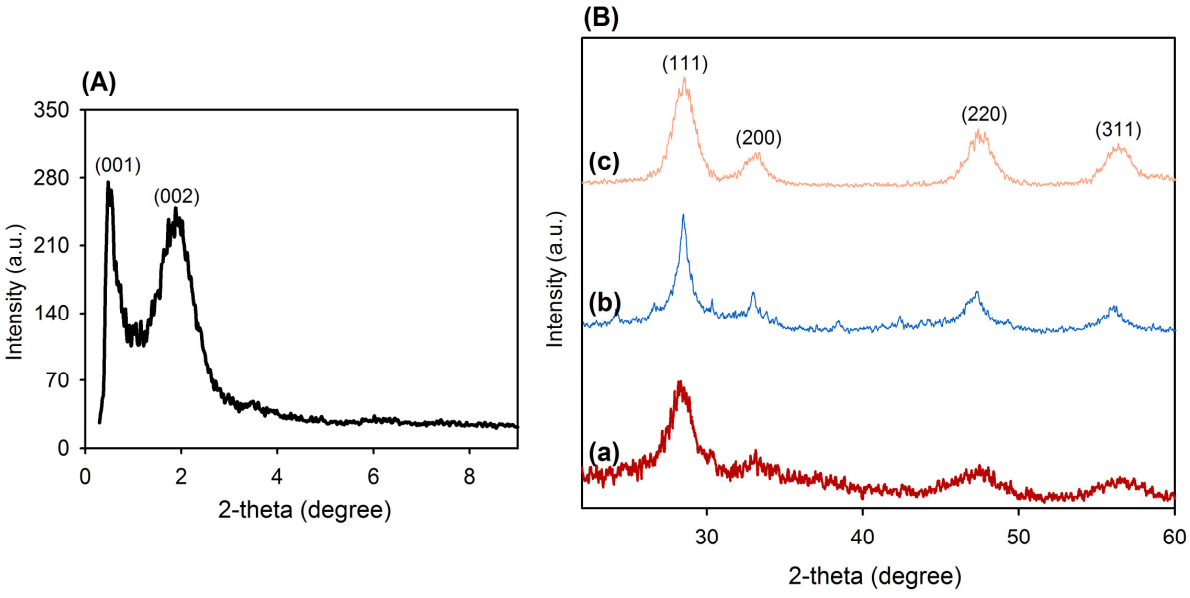

**Figure S1.** (A) Small-angle PXRD pattern of **C-1** and (B) wide-angle PXRD patterns of (a) **C2**, (b) **C3**, (c) **C4** shown in Table 1.

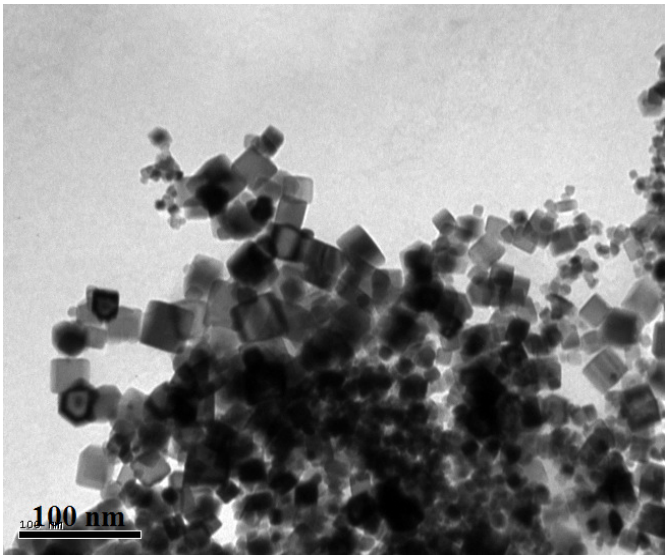


**Figure S2.** TEM image of $CeO_2$ nanoparticles synthesized without using hexamethylenediamine capping agent.

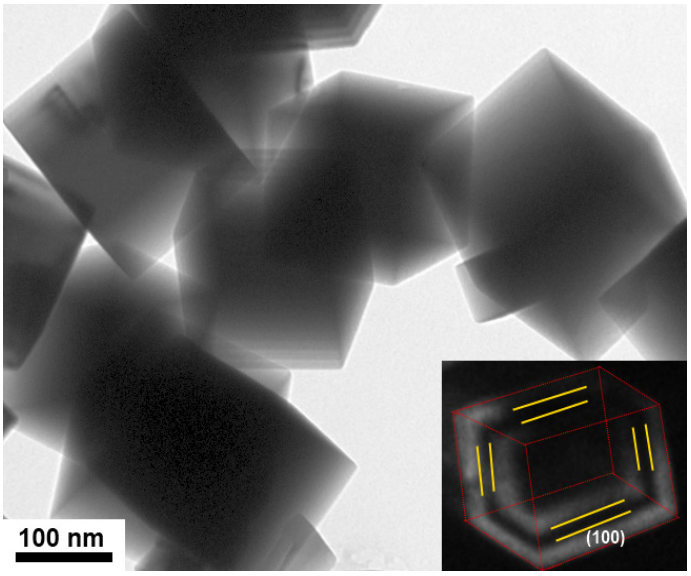

**Figure S3.** TEM image and inset of SAED pattern of $CeO_2$ nanocubes synthesized using HEA/Ce molar ratio of 1:2 (**C-5**).

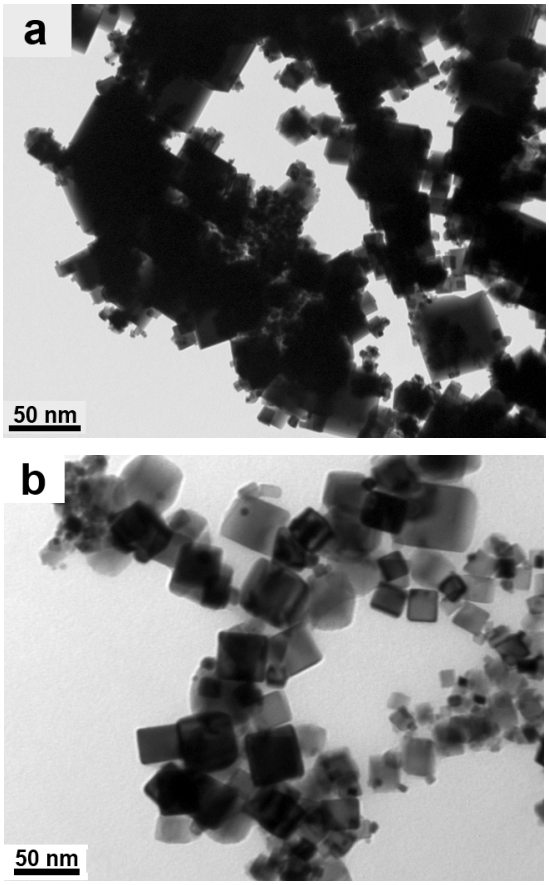


**Figure S4.** TEM images of $CeO_2$ nanoparticles synthesized at 180 $^{o}$C for each stage of the reaction time ($t$): (a) $t$ = 1 day, **C-6** and (b) $t$ = 2 days, **C-7**.

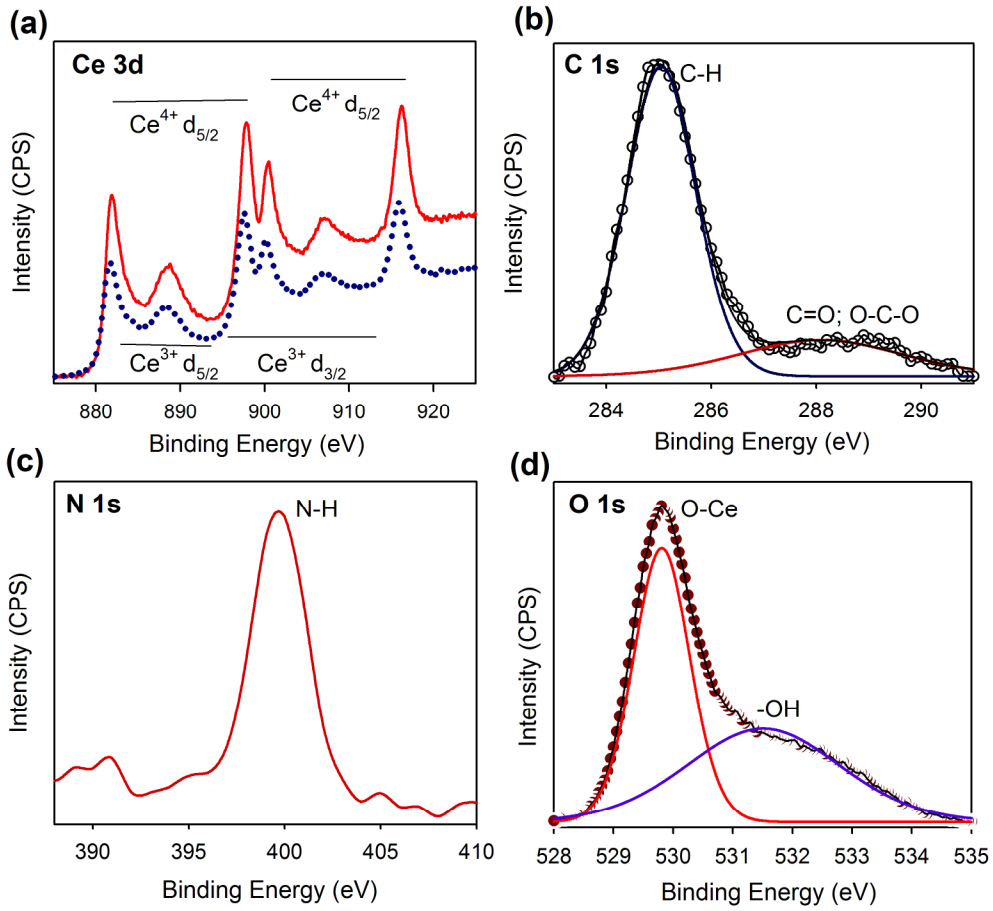


**Figure S5.** (a) Ce 3d XPS spectra of **C-5** (red line) and **C-7** (dotted blue line), and (b) C 1s, (c) N 1s, (d) O 1s XPS spectra of hexamethylenediamine-capped $CeO_2$ nanocubes (**C-5**).

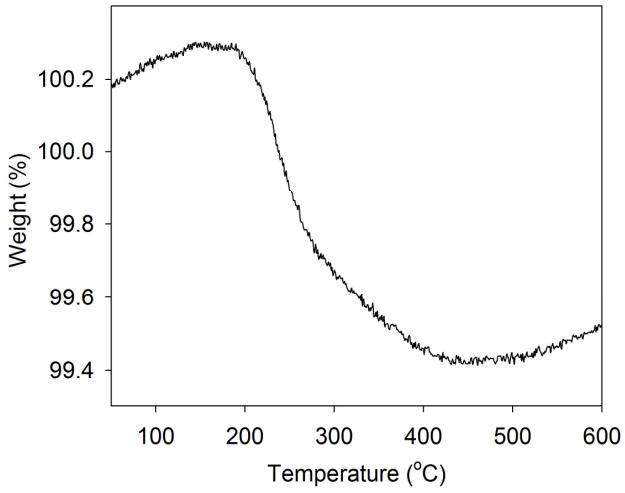


**Figure S6.** TGA curve of hexamethylenediamine-capped $CeO_2$ nanocubes (**C-5**).

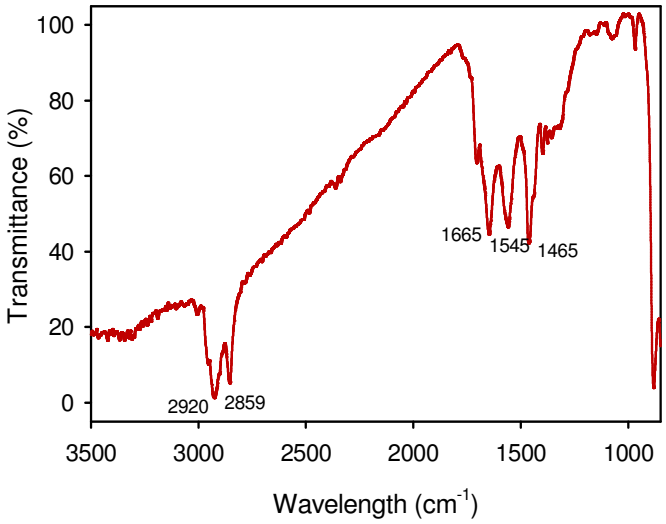


**Figure S7.** FTIR spectrum of hexamethylenediamine-capped $CeO_2$ nanocubes (**C-5**).

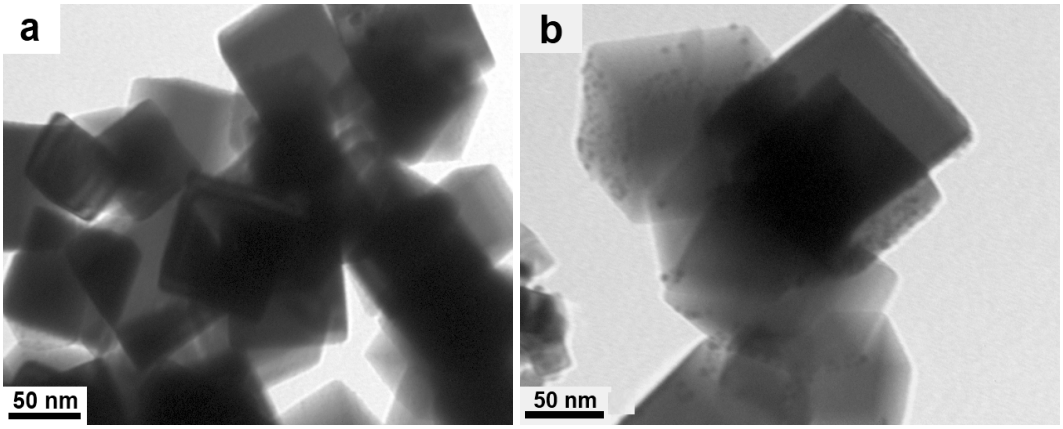


**Figure S8.** TEM images of single-crystalline $CeO_2$ nanocubes (**C-5**) and 9.1 wt.% $Cu/CeO_2$ hybrid nanostructures calcined at 550 $^oC$ for 3 h.

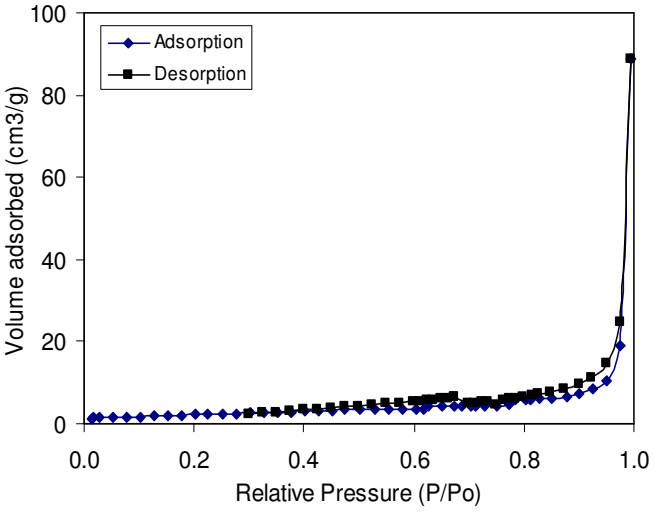


**Figure S9.** Nitrogen adsorption-desorption isotherms of calcined 9.1 wt.% $Cu/CeO_2$ nanohybrids.

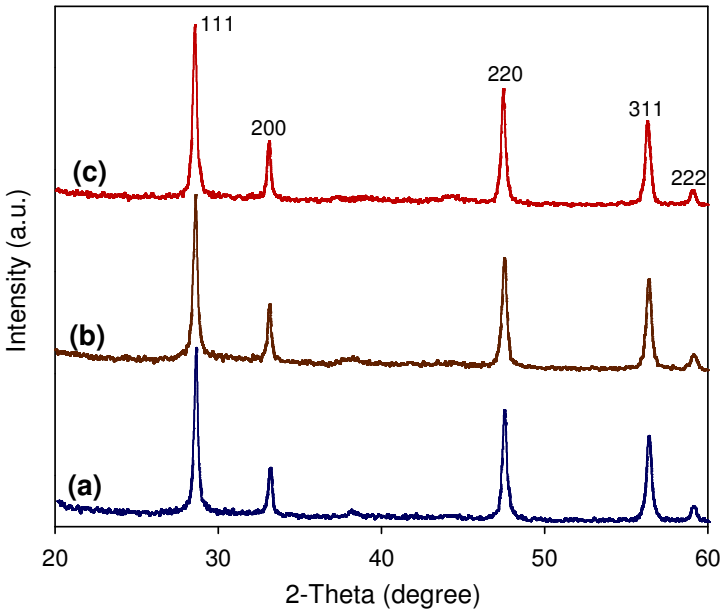


**Figure S10.** PXRD patterns of calcined $Cu/CeO_2$ nanohybrids with various Cu contents (*C*, wt.%): (a) *C* = 4.9 wt.%, (b) *C* = 9.1 wt.%, (c) *C* = 13.8 wt.%.

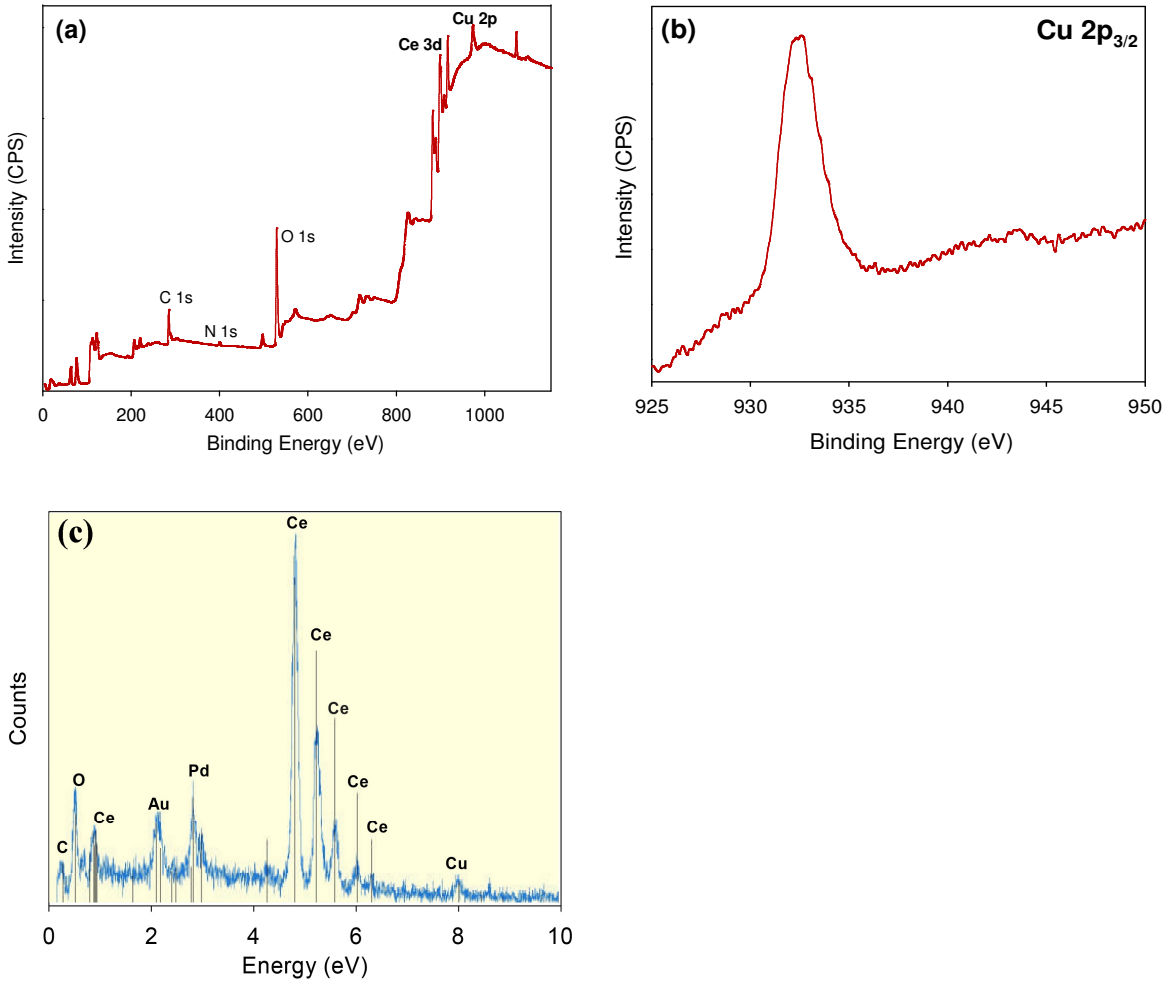


**Figure S11.** (a) Survey XPS spectrum, (b) Cu $2p_{3/2}$ XPS spectrum, and (c) EDX spectrum of calcined 9.1 wt.% $Cu/CeO_2$; amounts of Au and Pd were detected by sputter-coating with Au-Pd (5 nm).